Title: Porcine circovirus 2 particles use distinct binding modes for cellular attachment

Mobile title: Porcine circovirus 2 cellular recognition

Author Affiliation: Sonali Dhindwal[a], Bryant Avila[a], Reza Khayat[a,b,#]

a. Department of Chemistry and Biochemistry, The City College of New York, New York, NY 10031

b. Graduate Program in Biochemistry, The Graduate Center of the City University of New York, New York, NY 10016

Corresponding author: Reza Khayat, rkhayat@ccny.cuny.edu

19 **Classification:** Biological Sciences

20 **Abstract:**

21 Porcine circovirus 2 (**PCV2**) is the smallest autonomously replicating virus and thus defines the minimum amount
22 of genetic and biochemical information needed for infection. PCV2 infects nearly every tissue within its host,
23 and infections result in immunosuppression and subsequent death of the host. Infection is initiated via the
24 attachment of the PCV2 capsid to heparan sulfate and chondroitin sulfate B glycosaminoglycan (**GAG**) on the
25 surface of the cell. We demonstrate that the PCV2 capsid does not recognize the pyranose backbone of a GAG,
26 and solely interacts with the sulfates of GAG. We visualize the interaction between heparin sulfate, an analog
27 for heparan sulfate, and the PCV2 capsid using cryo-electron microscopy. The image reconstructions provide
28 the first example of an asymmetric distribution of heparin sulfate on the surface of a virus capsid. We
29 demonstrate that each subunit possesses six heparin sulfate binding sites, but binding at any site occludes
30 binding at the other five sites. The binding sites are defined by arginine, lysine, and polar amino acids. Mutation
31 of these arginine and lysine to alanine diminishes the binding capacity of the PCV2 to heparin sulfate. A third to
32 two-thirds of the binding sites (subunits) in each PCV2 is occupied by segments of one or multiple 12kDa heparin
33 sulfate chains –leaving the remaining subunits unliganded. We discuss the significance of the unliganded
34 subunits in the life cycle of PCV2.

35 Keywords. Circovirus, heparan sulfate, chondroitin sulfate B, glycosamino glycan, heparin sulfate, cellular
36 attachment, electron microscopy, symmetry expansion, focused classification.

37

38 **Significance statement:**

39 Studies describing the interaction between heparan sulfate (a cellular attachment factor) and non-enveloped
40 icosahedral viruses have adhered to the symmetry elements of the viral capsid. Here we provide the first
41 example where the interaction between heparan sulfate and a non-enveloped icosahedral virus does not follow
42 the symmetry elements of the viral capsid. We use cryo-electron microscopy, symmetry expansion, and focused
43 classification to visualize the interaction between the porcine circovirus 2 (PCV2) capsid. The non symmetric
44 interactions observed in our studies is likely to be true for all non-enveloped viruses, and more accurately
45 representative of what occurs during infection. We discuss how such interaction may be important to the life
46 cycle of PCV2.

47

48 **Introduction:**

49 Porcine circovirus 2 (**PCV2**) belongs to the *Circovirus* genus of the *Circoviridae* family (1). Members of this family
50 are non-enveloped viruses and possess a circular single stranded DNA (**ssDNA**) genome. Circoviruses are widely
51 distributed in nature and infect terrestrial, avian, and aquatic species in the animal kingdom (2). PCV2 infection
52 of swine causes Postweaning Multisystemic Wasting Syndrome (**PMWS**), which culminates in the
53 immunosuppression and death of the host from secondary infection. Autopsy of infected swine identifies PCV2
54 in nearly every tissue, indicating that it is a promiscuous virus (3). The promiscuous nature of PCV2 is further
55 exhibited by its ability to infect rodents and bovine in the wild, and BALB/c mice and human cells in the
56 laboratory (4-7). Remarkably, PCV2 is the smallest pathogenic virus capable of replicating in cells without the
57 need for additional viruses (8). The ~1.7knt ambisense PCV2 genome encodes for a replicase (ORF1) responsible
58 for the rolling circle replication of the genome, a capsid protein (ORF2) responsible for forming the capsid, and
59 an ORF3 and ORF4 which may be responsible for apoptosis and pathogenic nature of PCV2 (9-13). The PCV2
60 capsid is a T=1 icosahedron composed of 60-copies of the capsid protein with a fold that is the canonical viral
61 jelly-roll first observed for the capsid protein of tobacco bushy stunt virus (14-16).

62 Here we provide the first structural mechanism of cellular recognition by porcine circovirus using a combination
63 of cryo-electron microcopy, biochemistry, and site directed mutagenesis. PCV2 has been shown to initiate
64 cellular infection via attachment to the glycosaminoglycans (**GAG**s) heparan sulfate and chondroitin sulfate B
65 (17). Heparan sulfate and chondroitin sulfate B are ubiquitously expressed on mammalian cells and act as
66 attachment factors for a variety of macromolecules (18-20). Heparan sulfate is a 30 to 70 kDa polysaccharide
67 composed of multiple sulfated domains (**NS**) separated by unsulfated domains (**NA**). The NS domains are
68 composed of the repeating disaccharide L-Iduronic acid (**IdoA**) and D-Glucosamine (**GlcN**) connected via a 1→4
69 linkage (**Figure S1**). IdoA and GlcN can be sulfated on carbon 2 while GlcN can be additionally sulfated on carbon
70 6. Three to eight disaccharides constitute an NS domain. The NS domain is similar to heparin sulfate, and
71 heparin sulfate is routinely used as a reagent to study the interaction between the NS domains of heparan
72 sulfate and their interacting partners. It should be noted that heparin sulfate could be additionally sulfated on
73 carbon 3 of GlcN. The NA domains are composed of the repeating disaccharide N-Acetyl-D-Glusomaine (**GlcNAc**)
74 and D-Glucoronic acid (**GlcA**). Two to twelve disaccharides constitute an NA domain (**Figure S1**) (19).

75 Chondroitin sulfate B is composed of the repeating disaccharide N-Acetyl-Galactosamine (**GalNAc**) and IdoA
76 connected via a 1→3 linkage. GalNAc can be sulfated on carbon 4 (88% of pyranoses) and carbon 6 (5% or
77 pyranoses). IdoA can be sulfated on carbon 2 (7% or pyranoses) (20, 21).

78 In this study we use heparin sulfate as an analog for studying the interaction between heparan sulfate and PCV2.
79 We address the following questions: 1) what chemical moieties of heparin sulfate interact with PCV2, 2) where
80 are the heparin sulfate binding sites on the PCV2, 3) does binding of heparin sulfate follow the icosahedral
81 symmetry of the capsid, and 4) does PCV2 undergo conformational changes upon binding of heparin sulfate?

82 We demonstrate that PCV2 does not distinguish the backbone pyranose of GAGs, rather it interacts with the
83 sulfates. We determine that each capsid protein possesses six heparin sulfate-binding sites, and show that
84 binding of heparin sulfate to the icosahedral capsid does not adhere to the capsid's symmetry. To our
85 knowledge, this is the first example of an asymmetric distribution of heparin sulfate on an icosahedral virus.
86 Furthermore, we show that the subunits do not undergo a conformational change upon binding heparin sulfate.
87 We discuss the possible role of unliganded subunits in the life cycle of PCV2.

88 **Results:**

89 *The interaction between PCV2 and heparin sulfate is reversible and solely dictated by the sulfates*

90 To study the interaction between heparan sulfate and PCV2 we used an *in vitro* binding assay that involves
91 interacting PCV2 with chromatography sorbent conjugated to 15kDa porcine intestinal mucosa heparin sulfate.
92 Heparin sulfate is routinely used as an analog of heparan sulfate for studying the interaction between
93 macromolecules and heparan sulfate –the cellular attachment factor to initiate PCV2 infection (17-19). We
94 determined the amount of time necessary to interact PCV2 virus like particles (**VLP**, GenBank: ACA51584.1) with
95 the sorbent to achieve the maximum amount of binding to heparin sulfate (**Figure 1**). Two concentrations of
96 VLP were used (370 nM and 92 nM). Maximum binding occurred within 30 minutes for the lower concentration
97 of VLP, and within 3 hours for the higher concentration of VLP. We chose to use the higher concentration of
98 VLP (370 nM) for our subsequent studies because of its improved signal in our binding assays (**Figure S2).** We
99 then examined if the interaction was reversible by incubating the PCV2 bound sorbent with increasing

100 concentrations of 12kDa porcine intestinal mucosa heparin sulfate (**Figure 1**). Elution of PCV2 from the sorbent
101 demonstrates that the interaction is reversible.

102 We employed a competition assay to determine the chemical moieties of GAGs that PCV2 recognizes for cellular
103 attachment. The assays determine the effectiveness of different ligands to compete with the mentioned
104 chromatography sorbent for binding PCV2 (**Figure 1**). We examined the length and sulfation pattern of heparin
105 sulfate, the pyranose structure of the polysaccharide, and the branched nature of the polysaccharide chains.
106 The results demonstrate that while the efficiency of heparin sulfate dp6 (6-hexoses), dp10 (10-hexoses) and
107 dp20 (20-hexoses) to inhibit 15kDa heparin sulfate from binding to PCV2 increases, they are not nearly as
108 effective as dp36 (36-hexoses, 12kDa) heparin sulfate. A plausible explanation could be that there are multiple
109 weak binding sites on the PCV2 capsid, and that longer oligosaccharides have higher affinity to PCV2 because
110 they can bind to multiple sites concurrently. It has been shown that heparin sulfate fragments below dp18 are
111 helical, extended and rigid but become more bent with increasing size (22). Thus a dp6 and dp10 may bind to a
112 few binding sites on PCV2 that happen to follow their linear path, while the dp20 and dp36 heparin sulfate may
113 bend and bind to multiple sites on PCV2.

114 We then examined the ability of dextran sulfate (8kDa) to inhibit the interaction between PCV2 and the
115 chromatography sorbent. The dextran sulfate (8kDa) used in our studies is a highly branched polysaccharide,
116 with glucose repeating units connected via 1→4 linkages and branching points at 1→6. There are 2.8 sulfates
117 per glucose monomer for this product (personal communication with Alfa Aesar manufacturer). Dextran sulfate
118 is the ligand most efficient at inhibiting the interaction between PCV2 and 15kDa heparin sulfate (**Figure 1**).
119 Dextran, in contrast, appears to slightly enhance the affinity of the VLP for the sorbent (data not shown). This is
120 likely due to dextran acting as a crowding agent (23). The ability of dextran sulfate to inhibit PCV2 from binding
121 heparin sulfate while dextran slightly enhancing the interaction suggest that the sulfates are sufficient for
122 binding to PCV2, and that the backbone polysaccharide does not interact with PCV2.

123 Finally, we examined the ability of 1.6MDa hyaluronic acid (**HA**) and 41kDa chondroitin sulfate B
124 glycosaminoglycans to inhibit the interaction between PCV2 and 15kDa heparin sulfate. Hyaluronic acid
125 demonstrates no affinity for PCV2 (**Figure 1**). Hylauronic acid possesses a single carboxylate on each of its

126 repeating disaccharide units. The hydrogen bonds formed within and between its repeating disaccharides
127 produce stiff helical polysaccharide chains that entangle at very low concentrations (24). Thus, the carboxylate,
128 stiff, and entangled properties of HA may not provide the appropriate interface for PCV2 to bind. Chrondroitin
129 sulfate B (**CSB**) demonstrates affinity for PCV2, but this affinity is much lower when compared to that of heparin
130 sulfate. This may be because of the lower sulfate content of CSB (an average of one sulfate per repeating
131 disaccharide) when compared to heparin sulfate (an average of three sulfates per repeating disaccharide). The
132 increased flexibility of CSB, as compared to the stiff nature of heparin sulfate, may allow CSB to bind additional
133 binding sites on the PCV2 capsid despite its low sulfate content (25).

134 *Distribution of heparin sulfate on PCV2 does not follow the icosahedral symmetry of the capsid*

135 To identify the binding sites of heparin sulfate on PCV2 we determined the cryo-EM image reconstruction of
136 PCV2 in the absence and presence of 12kDa (dp36) porcine intestinal mucosa heparin sulfate at pH 7. The
137 unliganded PCV2 image reconstruction, with imposed icosahedral symmetry, at a nominal resolution of 3.3Å is
138 similar to that reported by Liu et al. **(Figure 2)** (26). The atomic structures from the two reconstructions share
139 92.6% sequence identity and superpose with a root-mean-square deviation (**RMSD**) of 0.437Å. We generated
140 three cryo-EM image reconstructions of PCV2 in complex with heparin sulfate using a single data set. The image
141 reconstruction with imposed icosahedral symmetry at 2.8Å resolution is indistinguishable from the unliganded
142 image reconstruction described above, suggesting that the interaction between PCV2 and heparin sulfate may
143 not follow icosahedral symmetry, or that heparin sulfate was displaced during sample preparation. Similarly,
144 the refined atomic model is indistinguishable from the atomic model of the unliganed image reconstruction –the
145 RMSD for the two structures is 0.268Å. However, plotting the atomic displacement parameters (**ADP**) onto the
146 structures suggests that the heparin sulfate-liganded image reconstruction may be more dynamic (**Figure 2**).
147 We then generated an asymmetric image reconstruction of the complex to 3.2Å resolution. Close inspection of
148 the image reconstruction at low contour levels identified molecular envelopes on the surface of PCV2 that could
149 not be accounted for by the PCV2 atomic coordinates; however, these envelopes are too weak to confidently
150 label as heparin sulfate. We postulated that if each subunit possessed multiple binding sites for heparin sulfate
151 but only one site could be occupied per subunit then each capsid might be composed of a unique combination

152 of subunits liganded to heparin sulfate; thus, any averaging strategy could eliminate the molecular envelope of
153 heparin sulfate. To test this possibility, we employed the expand symmetry capability of Relion on the
154 alignment parameters from the image reconstruction where icosahedral symmetry was imposed. The
155 consequence of this strategy is to align the projections from all subunits to one another. We then used Frealign
156 to perform masked classification of a subunit (27-29)**.** Seven of the ten classes identified molecular envelopes
157 that could not be seen in the original image reconstruction (**Figure 3**). To generate a difference map for each
158 class average we subtracted from the class average an image reconstruction generated using the same number
159 of particles as the class average –these particles were randomly selected from the symmetry expanded data set.
160 The difference peaks were low-pass filtered to 7Å resolution to smoothen the shapes.

161 *Mutation of Arg/Lys residues defining the heparin sulfate binding sites diminish the affinity of the capsid for*
162 *heparin sulfate*

163 A total of seven difference peaks with strengths greater than 27-sigma are observed for the 10 classes (**Figure 3**).
164 We used 27-sigma as the criteria to remove small and spurious difference density peaks. These peaks may
165 correspond to segments of the 12kDa heparin sulfate molecule incubated with PCV2. We note that the
166 amorphous shapes of these peaks may suggest that heparin sulfate uses multiple binding modes/poses to bind
167 to the capsid. Indeed, heparin sulfate is known to use multiple binding modes/poses to interact with proteins
168 (30). We modeled segments of heparin sulfate as rigid bodies into the difference peaks to see if the models
169 were chemically reasonable. We then examined if mutation of the Arg and Lys amino acids that interact with
170 the sulfates in our models diminished the mutant VLP's affinity for heparin sulfate. Class 1 (11% of subunits)
171 does not possess a difference peak and thus represents an unliganded subunit. The difference peak for class 2
172 (9% of subunits) is located near Arg73 and Lys132 of the same subunit. Mutation of Arg73 to Ala diminishes
173 capsid-heparin sulfate affinity to 63% of wild type, whereas mutation of Lys132 to Ala abolishes capsid assembly.
174 A four-hexose segment of heparin sulfate can be modeled into this difference peak (**Figure 4**). The difference
175 peak for class 3 (9% of subunits) is located near Lys58 and Arg59, but is too small to accommodate heparin
176 sulfate; thus, we interpret this class to represent an unliganded subunit. The difference peak for class 4 (11% of
177 subunits) is near Arg89, and next to the icosahedral 2-fold axis of symmetry. Mutation of Arg89 to Ala

178 diminishes capsid-heparin sulfate affinity to 48% of wild type. A three-hexose segment of heparin sulfate can be
179 modeled into this density (**Figure 4**). The difference peak for class 5 (10% of subunits) is extremely week; thus,
180 we interpret this class to represent an unliganded subunit. The difference peak for class 6 (9% of subunits) runs
181 between adjacent facets. It is located near Arg186 and Lys227 of the adjacent subunit. Mutation of Arg186 to
182 Ala diminishes the capsid-heparin sulfate affinity to 76% of wild type, whereas mutation of Lys227 to Ala
183 abolishes capsid assembly. A five-hexose segment of heparin sulfate can be modeled into this difference peak.
184 A number of hydrogen bonds are possible between the sulfates of heparin and the side chains of Thr131,
185 Tyr138, and Ser86 (**Figure 4**). The difference peak for class 7 (14% of subunits) is distal to Arg/Lys, but a five-
186 hexose segment of heparin sulfate modeled into the difference peak suggests that hydrogen bonds can form
187 between the sulfates of heparin and the side chains of Asn128, Gln188, and the three Tyr173 at the icosahedral
188 3-fold axis (**Figure 4**). The difference peak for class 8 (12% of subunits) is also very weak; therefore, we interpret
189 this class as an unliganded subunit. The difference peak for class 9 (7% of subunits) is located near Arg73 and
190 Lys132 of a subunit. A three-hexose segment of heparin sulfate modeled into this difference peaks can form
191 additional hydrogen bonds between heparin's sulfates and the side chains of Asn128 and Gln188 (**Figure 4**). The
192 difference peak for class 10 (8% of subunits) is located near the icosahedral 5-fold axis, and surrounded by Lys58
193 and Arg59 of one subunit and Lys63 of a neighboring subunit. A sulfate was also observed at this location in the
194 crystal structure of PCV2 (31). Mutation of either Lys58 or Arg59 to Ala diminishes PCV2-heparin sulfate
195 interaction to 65%, while mutation of Lys63 diminishes the affinity to 38%. A two-hexose segment of heparin
196 sulfate can be modeled into this density (**Figure 4**).

197 *Occupied heparin binding sites cluster on the surface of VLPs*

198 We used Relion's symmetry operators to map the class that each subunit is assigned to onto the VLP to generate
199 composite molecular envelopes representing each VLP bound to heparin sulfate (**Figure 5**). The composite
200 molecular envelopes consist of icosahedral facets with zero to multiple binding sites occupied. The distribution
201 of binding sites occupied per VLP, for the data set as a whole, follows a Gaussian distribution with a minimum of
202 20 sites bound, a mode of 36 sites bound, and a maximum of 47 sites bound (**Figure S4**). The occupied binding
203 sites cluster on each VLP, and indeed some appear to follow a linear trajectory that may represent a single

204 heparin sulfate chain (**Figure 5**). The molecular envelope of each image reconstruction is of high enough quality
205 for us to refine the atomic models with little ambiguity. Refining the atomic model, generated from the image
206 reconstruction with imposed icosahedral symmetry, into each of the seven classes does not identify any
207 significant movement that could be associated with a conformational change upon binding of heparin sulfate.
208 The largest RMSD between two subunits is 0.313Å.

209 **Discussion**

210 Heparin sulfate is routinely used as an analog of heparan sulfate to study protein-heparan sulfate interaction
211 (19). Our biochemical studies demonstrate that the interaction between PCV2 capsid and heparin sulfate is
212 heavily reliant on the length of the polysaccharide chain, with longer chains exhibiting a greater affinity for the
213 capsid. This suggests that heparin sulfate may bind to the capsid via multiple weak binding sites. Our
214 biochemical data further suggests that the interaction is solely driven by the sulfate moieties on heparin sulfate
215 and chondroitin sulfate B. Our structural data identifies six binding sites per PCV2 capsid protein. Amino acids
216 in these binding sites properly positioned to interact with heparin's sulfate moieties include Arg, Lys, Asn, Gln,
217 Ser, Thr, and Tyr. Mutations of the Arg and Lys amino acids to Ala diminish the capsid's affinity for heparin, and
218 thus provide biochemical support for the structural data. Mapping the occupied binding sites onto the VLP
219 generates representative molecular envelopes for each VLP. These envelopes demonstrate that heparin sulfate
220 binds to patches on the surface of the capsid rather than symmetrically as has been demonstrated for a number
221 of other viruses. This is because prior structural studies of icosahedral viruses in complex with heparin sulfate
222 utilized averaging techniques that may have eliminated the asymmetric distribution of heparin sulfate on the
223 capsid surface (32-36). The packing of capsids into a crystal for X-ray crystallography inherently imposes the
224 averaging of structures (37). Similarly, cryo-EM image reconstructions with imposed icosahedral symmetry
225 average non-icosahedral entities to symmetric structures with reduced occupancy or amorphous blobs (e.g. the
226 molecular envelope of vial genomes). However, the use of symmetry expansion, focused classification, and back
227 mapping forgo such averaging techniques to provide a more detailed analysis of the specimen under study.

228 The unliganded patches of capsid protein subunits may be important for subsequent steps of infection. Misinzo
229 et al. 2006 demonstrated that PCV2 is capable of infecting CHO mutant cells that are deficient in expressing

230 glycosaminoglycans on their surface –suggesting that additional macromolecules on the surface of the cell
231 interact with unliganded PCV2 to initiate infection. Thus it may be possible that the unliganded subunits interact
232 with these additional macromolecules in the next stage of infection. Misinzo et al., 2008 demonstrated that the
233 serine protease inhibitor [4-(2-aminotheyl) benzenesulfonyl fluoride hydrochloride] (**AEBSF**) completely blocked
234 PCV2 infection of PK-15 cells by inhibiting capsid disassembly in the endosome-lysosome system –suggesting
235 that digestion of PCV2 subunits by a cellular endosome-lysosome serine protease may be necessary for
236 infection. Indeed, the PROSPER Protease specificity prediction server identifies a number of Cathepsin G (a
237 lysosomal serine protease) digestion sites in the capsid protein sequence. Two of these sites are on the surface
238 of the capsid and become inaccessible when heparin sulfate is modeled into the difference peaks identified in
239 this study. The attachment of heparan sulfate to a PCV2 subunit may create a steric hindrance for such a
240 protease to help disassemble the capsid; thus, it would make sense for some subunits to be unliganded to
241 heparan sulfate so that the subunits could be hydrolyzed by such a serine protease.

242 In conclusion, we demonstrate that PCV2 capsids recognize the sulfates of GAGs rather than the backbone
243 pyranoses, that subunits possess six binding sites capable of binding heparin sulfate but only one site is occupied
244 per subunit, that not all binding sites are occupied, that the binding of heparin sulfate to the capsid does not
245 adhere to the icosahedral symmetry of the capsid, and that binding of heparin does not induce a conformational
246 change in the capsid but may affect its dynamics.

247

248 **Materials and Methods**

249 *PCV2 VLP expression and purification*

250 The codon sequence for the PCV2 capsid protein (GeneBank ACN59889.1) was optimized by GenScript for
251 Baculovirus expression system. GenScript also generated the Baculovirus stock used in these studies.
252 *Trichoplusia ni* insect cells were propagated in ESF921 medium (Expression System) and infected with the
253 Baculovirus at an MOI of 0.1. Cells were grown for 5 days till 70% had lysed according to Trypan blue staining.

254 PCV2 VLP was purified from the nucleus of the infected cells. Cells from 500ml of media were gently centrifuged
255 at 800xg for 10 minutes at 4°C. The cell pellet was suspended and lysed in 20mM 4-(2-hydroxyethyl)-1-
256 piperazineethanesulfonic acid (HEPES) pH 7.5, 250mM Sodium Chloride (NaCl), 2mM Magnesium Chloride
257 (MgCl), 1mM Tris(2-carboxyethyl)phosphine hydrochloride (TCEP), 1% (v/v) NP-40, and placed on a revolver at
258 4°C for 30 minutes. The lysate was centrifuged for 30 minutes, 720xg, at 4°C to pellet the nuclei. The nuclei
259 were suspended in 20mM HEPES, 500mM NaCl, 2mM $MgCl_2$, 0.2mM TCEP, 2mM Deoxycholate, salt activated
260 nuclease (Sigma-Aldrich) and lysed using a sonicator. The lysate was centrifuged at 28,000xg for 30 minutes at
261 4°C. The supernatant was overlaid on a 30% sucrose cushion and centrifuged at 184,000xg, 11°C, 2.5 hours
262 using a 45Ti rotor. The pellet was suspended in 2ml of nucleus lysis buffer and processed on a discontinuous 20
263 to 70% sucrose gradient. The gradient was centrifuged using a SW40 rotor at 160,000xg, 4°C, and 18 hours. The
264 fraction containing the VLP was visually identified using light scattering and SDS-PAGE. The fraction was dialyzed
265 overnight in 20mM HEPES 7.0, 250mM NaCl, 0.2mM TCEP, and 2mM ethylenediaminetetraacetate (EDTA).
266 Samples were concentrated to 370nM using a 100kDa MWCO ultrafiltration device (Pall Corporation), and
267 stored at 4°C.

268 *Sequence analysis*

269 The sequence identity between the ORF2 of GenBank entry ACA51584.1 and Stoon-1010 (17) was determined
270 using the EMBOSS Needle server at EMBL-EBI.

271 *Binding studies*

272 Heparin HyperD™ M Affinity Chromatography Sorbent (Pall Corporation) is conjugated to 15kDa porcine
273 intestinal mucosa heparin sulfate. HyperD™ M was washed and equilibrated with 20mM HEPES 7.0, 250mM
274 NaCl, 0.1mM TCEP, 2mM EDTA and allowed to settle to the bottom of the tube. Each reaction contained 2μl of
275 settled HyperD™ M and the indicated amount of VLP (see below). Samples were incubated at 20°C for the
276 indicated amount of time (see below) on a revolver to allow PCV2 to bind to the sorbent. The HyperD™ M
277 sorbent was gently pelleted at 100xg for 30s, washed two-times using the equilibration buffer, suspended in
278 water, and processed using SDS-PAGE. The PAGE was stained using InstantBlue™ from Expedeon, and band
279 intensities were quantitated using the Li-Cor Odyssey Blot Imager equipped with Image Studio™ Software
280 version 5.0. The washes did not remove VLP from the sorbent (data not shown).

281 Kinetic binding assays: 4μl of VLP at concentrations of 370 nM and 92.5 nM were incubated with 2μl of
282 HyperD™ M for 5 seconds (**s**), 10s, 30s, 1 minute (m), 5m, 10m, 20m, 1 hour (h), 3h and 24h on a revolver at
283 20°C. The sorbent was processed as described above.

284 Elution assays: VLP bound to HyperD™ M sorbent (as described above) was incubated with increasing
285 concentrations of porcine intestinal mucosa heparin sulfate (see below) for 3 hours at 20°C. The bound VLP was
286 quantitated as described above.

287 Competition assays: GAG reagents were incubated with PCV2 at 20°C for 3h prior to performing the binding
288 assay. VLP and GAG were incubated for 3h with the HyperD™ M sorbent. The sorbent was processed as
289 described above.

290 *Glycosaminoglycans and polysaccharide source*

291 Heparin sulfate oligosaccharides (HO06, HO10, HO20), and chondroitin sulfate B (DS01) were purchased from
292 Galen laboratories, and dissolved in water. Porcine intestinal mucosa heparin sulfate (average molecular weight
293 12kDa) was purchased from JT Baker, hyaluronic acid and dextran sulfate 8kDa from Alfa Aesar. All reagents
294 were used within 48 hours after being dissolved in the VLP dialysis buffer. Concentrations were calculated
295 based on the disaccharide molecular weight of 659 g/mol for heparin sulfate, 551 g/mol for chondroitin sulfate
296 B, 389 g/mol for Hyaluronic acid, and 728 g/mol for dextran sulfate 8kDa. Samples were stored at 4°C.

297 *Electron microscopy and image reconstruction*

298 Ultrathin carbon film on Lacey Carbon support film (TedPella, 01824) were used for cryo-electron microscopy.
299 Grids were glow discharged using a PELCO easiGlow™ for 30 seconds. Samples (4μl) were adsorbed to the grid
300 for 15 seconds, blotted with a force of 2 for 6 seconds, and plunge frozen into liquid ethane using an FEI Mark IV
301 vitrobot. Data for the unliganded PCV2 was collected using a side entry FEI Titan Halo with the Leginon software
302 (38). Images were collected at a calibrated magnification of 45,871x on a Gatan K2 camera operating in
303 counting mode. Cryo-EM grids for the PCV2 liganded to heparin sulfate were prepared by incubating 20μl of the
304 VLP with 7μl of 60mg/ml 12 kDa heparin sulfate for 3 hours. The mixture was then incubated with 2μl of
305 HyperD™ M sorbent for 3 hours at 20°C on a revolver to remove VLP that was not bound to heparin sulfate.
306 Cryo-EM grids were prepared as described for the unliganded PCV2. Data for the heparin sulfate liganded PCV2
307 was collected on a Titan Krios with the Leginon software. Images were collected at a calibrated magnification of
308 45,871x on a Gatan K2 camera that follows a GIF Quantum Energy Filter with a slit width of 15eV. Data
309 collection parameters for both data is reported in **Table 1**.

310 Motion correction was performed using the MotionCor2 package (39). The first frame of each movie was
311 discarded during the alignment. With the exception of a patch 5 option, the default options were used for the
312 alignment and dose weighting. Particles were automatically detected using Gautomatch and per-particle
313 contrast transfer function (**CTF**) estimation was performed on the aligned micrographs using Gctf (40). Briefly,
314 particles were extracted from the dose-weighted micrographs using the coordinates identified by Gautomatch.
315 Reference free 2D classification with a diameter of 250Å and default Relion 2.0 parameters were used to discard
316 bad particles (29). The PCV2 crystal structure (PDB entry 3R0R) was used to generate a 60Å resolution initial
317 model for 3D classification with default Relion 2.0 parameters and C1 symmetry. The 3D class with the highest
318 resolution image reconstruction was used for further refinement using I1 symmetry. Default parameters were
319 used for the refinement and postprocessing.

320 The procedure for processing the PCV2 liganded to heparin sulfate data is identical to that of the unliganded
321 data; however, an additional 3D refinement was performed using C1 symmetry following 3D classification. For
322 the masked classification, the refinement parameters for 3D refinement with I1 symmetry of 13,600 particles

323 were further processed using the *relion_particle_symmetry_expand* program of Relion 2.0. A 25Å resolution
324 volume of a subunit was generated using the *molmap* function of UCSF Chimera (41) . The mask was manually
325 moved outward to include area peripheral to the capsid in case heparin sulfate may be present on the surface of
326 the capsid. The alignment parameters and images were converted to a format for Frealign using the
327 *relion_preprocess* function of Relion and the conversion script provided by the Frealign authors. Twenty rounds
328 of masked classification (10 classes) without alignment were performed (28, 42).

329 Difference maps were calculated using the *vop* function of UCSF Chimera (41). The image reconstruction from
330 each class was subtracted from an image reconstruction generated using the same number of particles
331 randomly selected from the entire data. The image reconstructions from randomly selected particles were
332 visually indistinguishable from the icosahedrally averaged image reconstruction.

333 The difference peaks for each class were mapped onto the symmetrized image reconstruction using the
334 symmetry operators (I1) of Relion used during the symmetry expansion process. These composite volumes were
335 generated and visualized using the UCSF Chimera package.

336 *Structure refinement*

337 The reported crystal structure of PCV2 (31) was manually docked into the symmetrized image reconstructions
338 using UCSF Chimera. The resulting coordinates were iteratively refined using *phenix.real_space_refine* with
339 noncrystallographic symmetry constraints applied, and manual fitting with Coot (43, 44).

340 Hepairn sulfate molecules (PDB entries 3IRI, 3IRJ, 3IRK, and 3IRL) were treated as rigid bodies and manually
341 fitted into the difference peaks of the six classes described above. The capsid protein subunit pertaining to
342 these molecular envelopes were further refined using manual fitting and *phenix.real_space_refine,* without
343 noncrystallocgraphic symmetry.

344 *Mutagenesis and binding efficiency*

345 Single point mutants of the PCV2 capsid were made to the consensus sequence construct described in Khayat et
346 al. 2011. Briefly, this construct possesses a hexahistidine and a thrombin cleavage site at the N-terminus in lieu
347 of the forty-two amino acids in the GeneBank ACN59889.1. The remaining amino acid sequence is identical.

348 Mutations were made using the New England Biolabs Inc. site directed mutagenesis kit. Sequences were
349 confirmed using the services of Genewiz. Proteins were purified as previously described (45). Virus like particles
350 (**VLP**s) were assembled by mixing equal volumes of the capsid protein at 37 μM with 12% polyethylene glycol
351 3350, 5% isopropanol, and 0.6M Ammonium Citrate pH 5.0 at 4°C overnight. VLPs form crystals in this solution.
352 The crystals were pelleted via centrifugation at 14,000xg for 10minutes at 4°C. The pellet was suspended in
353 0.3M HEPPS 9.0, 0.6M NaCl, and 5mM β-mercaptoethanol (β-Me) and processed through a HiPrep 16/60
354 Sephacryl S-500 HR (GE Healthcare Life Sciences) equilibrated with 20mM HEPPS 9.0, 0.6M NaCl, and 5mM β-
355 Me. The eluted peak was concentrated using a 100kDa MWCO ultrafiltration device (Pall Corporation) and
356 assessed with negative stained electron microscopy. Briefly, 3 μl of the sample was applied to a glow discharged
357 carbon coated 400 mesh copper grid (TedPella, 01814-F) and stained with 2% Uranyl Formate. Images were
358 collected using a JEOL JEM-1230 microscope operating at 120kV and equipped with a Gatan US-4000 charge
359 coupled device.

360 Binding studies were performed as described above. The interaction between the sorbent and 370 nM of VLP
361 were measured three times to generate error bars.

362

363 **Acknowledgement**

364 Funds responsible for supporting these studies were provided by NIH National Institute of General medical
365 Sciences and National institute of Allergy and Infectious Diseases (5SC1AI114843) and by Grant Number
366 5G12MD007603-30 from the National Institute on Minority Health and Health Disparities. Some of this work was
367 performed at the Simons Electron Microscopy Center and National Resource for Automated Molecular
368 Microscopy located at the New York Structural Biology Center, supported by grants from the Simons Foundation
369 (349247), NYSTAR, and the NIH National Institute of General Medical Sciences (GM103310). The authors would
370 like to acknowledge the Imaging Facility of CUNY Advanced Science Research Center for instrument use,
371 scientific and technical assistance.

372 The image reconstructions and atomic coordinates have been deposited into the EMDB and PDB respectively.

373 Accession codes (EMDB/PDB) are: Unliganded image reconstruction (8939/6DZU); symmetrized liganded image

374 reconstruction (8969/6E2R); Class 02 (8970/6E2X); Class 04 (8971/6E2Z); Class 06 (8972/6E30); Class 07

375 (8973/6E32); Class 09 (8974/6E34); Class 10 (8975/6E39).

376

377 **References**

378 1. Todd D (2000) Circoviruses: Immunosuppressive threats to avian species: A review. *Avian Pathology*
379 29(5):373–394.

380 2. Lorincz M, Csagola A, Farkas SL, Szekely C, Tuboly T (2011) First detection and analysis of a fish circovirus.
381 *Journal of General Virology* 92(8):1817–1821.

382 3. Meng X-J (2013) Porcine Circovirus Type 2 (PCV2): Pathogenesis and Interaction with the Immune
383 System. *Annu Rev Anim Biosci* 1(1):43–64.

384 4. Hattermann K, et al. (2004) Infection studies on human cell lines with porcine circovirus type 1 and
385 porcine circovirus type 2. *Xenotransplantation* 11(3):284–294.

386 5. Pinheiro ALBC, et al. (2013) Research in Veterinary Science. *Research in Veterinary Science* 94(3):764–
387 768.

388 6. Kiupel M, et al. (2001) Viral replication and lesions in BALB/c mice experimentally inoculated with porcine
389 circovirus isolated from a pig with postweaning multisystemic wasting disease. *Veterinary Pathology*
390 38(1):74–82.

391 7. Halami MY, Freick M, Shehata AA, Müller H, Vahlenkamp TW (2014) Veterinary Microbiology. *Vet*
392 *Microbiol* 173(1-2):125–131.

393 8. Ramamoorthy S, Meng X-J (2009) Porcine circoviruses: a minuscule yet mammoth paradox. *Anim Health*
394 *Res Rev* 10(1):1–20.

395 9. Liu J, Chen I, Kwang J (2005) Characterization of a previously unidentified viral protein in porcine
396 circovirus type 2-infected cells and its role in virus-induced apoptosis. *J Virol* 79(13):8262–8274.

397 10. Liu J, Chen I, Du Q, Chua H, Kwang J (2006) The ORF3 protein of porcine circovirus type 2 is involved in
398 viral pathogenesis in vivo. *J Virol* 80(10):5065–5073.

399 11. Chaiyakul M, Hsu K, Dardari R, Marshall F, Czub M (2010) Cytotoxicity of ORF3 proteins from a
400 nonpathogenic and a pathogenic porcine circovirus. *J Virol* 84(21):11440–11447.

401 12. Lv Q, Guo K, Wang T, Zhang C, Zhang Y (2015) Porcine circovirus type 2 ORF4 protein binds heavy chain
402 ferritin. *J Biosci* 40(3):477–485.

403 13. Tischer I, Gelderblom H, Vettermann W, Koch MA (1982) A very small porcine virus with circular single-
404 stranded DNA. *Nature* 295(5844):64–66.

405 14. Harrison SC, Olson AJ, Schutt CE, Winkler FK (1978) Tomato bushy stunt virus at 2.9 Å resolution.

406 15. Khayat R, johnson JE (2011) Pass the jelly rolls. *Structure* 19(7):904–906.

407 16. Crowther RA, Berriman JA, Curran WL, Allan GM, Todd D (2003) Comparison of the structures of three
408 circoviruses: chicken anemia virus, porcine circovirus type 2, and beak and feather disease virus. *J Virol*
409 77(24):13036–13041.

410 17. Misinzo G, Delputte PL, Meerts P, Lefebvre DJ, Nauwynck HJ (2006) Porcine circovirus 2 uses heparan
411 sulfate and chondroitin sulfate B glycosaminoglycans as receptors for its attachment to host cells. *J Virol*
412 80(7):3487–3494.

413 18. Sarrazin S, Lamanna WC, Esko JD (2011) Heparan Sulfate Proteoglycans. *Cold Spring Harbor Perspectives*
414 *in Biology* 3(7):a004952–a004952.

415 19. Rabenstein DL (2002) Heparin and heparan sulfate: structure and function. *Nat Prod Rep* 19(3):312–331.

416 20. Mizumoto S, Yamada S, Sugahara K (2015) ScienceDirectMolecular interactions between chondroitin.
417 *Curr Opin Struct Biol* 34:35–42.

418 21. Burzava ALS, et al. (2017) Affinity Binding of EMR2 Expressing Cells by Surface-Grafted Chondroitin
419 Sulfate B. *Biomacromolecules* 18(6):1697–1704.

420 22. Khan S, Gor J, Mulloy B, Perkins SJ (2010) Semi-Rigid Solution Structures of Heparin by Constrained X-ray
421 Scattering Modelling: New Insight into Heparin–Protein Complexes. *J Mol Biol* 395(3):504–521.

422 23. Laurent TC (1995) An early look at macromolecular crowding. *Biophysical Chemistry* 57(1):7–14.

423 24. Necas J, Bartosikova L, Brauner P, Kolar J (2008) Hyaluronic acid (hyaluronan): a review. *Veterinarni*
424 *Medicina* 53(8):397–411.

425 25. Thelin MA, et al. (2013) Biological functions of iduronic acid in chondroitin/dermatan sulfate. *FEBS J*
426 280(10):2431–2446.

427 26. Liu Z, Guo F, Wang F, Li T-C, Jiang W (2016) 2.9 A˚ Resolution Cryo-EM 3D Reconstruction of Close-Packed
428 Virus Particles. *Structure/Folding and Design* 24(2):319–328.

429 27. Ilca SL, et al. (1AD) Localized reconstruction of subunits from electron cryomicroscopy images of
430 macromolecular complexes. *Nature Communications* 6:1–8.

431 28. Lyumkis D, Brilot AF, Theobald DL, Grigorieff N (2013) Journal of Structural Biology. *J Struct Biol*
432 183(3):377–388.

433 29. Scheres SHW (2012) RELION: implementation of a Bayesian approach to cryo-EM structure
434 determination. *J Struct Biol* 180(3):519–530.

435 30. Xu D, Esko JD (2014) Demystifying Heparan Sulfate–Protein Interactions. *Annu Rev Biochem* 83(1):129–
436 157.

437 31. Khayat R, Lander GC, johnson JE (2010) An automated procedure for detecting protein folds from sub-
438 nanometer resolution electron density. *J Struct Biol* 170(3):513–521.

439 32. Spillmann D (2001) Heparan sulfate: anchor for viral intruders? *Biochimie* 83(8):811–817.

440 33. Fry EE, et al. (1999) The structure and function of a foot-and-mouth disease virus-oligosaccharide
441 receptor complex. *EMBO J* 18(3):543–554.

442 34. O'Donnell J, Taylor KA, Chapman MS (2009) Adeno-associated virus-2 and its primary cellular receptor—
443 Cryo-EM structure of a heparin complex. *Virology* 385(2):434–443.

444 35. Xie Q, et al. (2017) The 2.8 A˚ Electron Microscopy Structureof Adeno-Associated Virus-DJ Boundby a
445 Heparinoid Pentasaccharide. *Molecular Therapy: Methods & Clinical Development* 5:1–12.

446 36. Zhang W, Heil M, Kuhn RJ, Baker TS (2005) Heparin binding sites on Ross River virus revealed by electron
447 cryo-microscopy. *Virology* 332(2):511–518.

448 37. johnson JE, Rueckert RR (1997) *Structural Biology of Viruses* eds Chiu W, Burnett RM (New York).

449 38. Suloway C, et al. (2005) Automated molecular microscopy: the new Leginon system. *J Struct Biol*
450 151(1):41–60.

451 39. Zheng SQ, et al. (2017) MotionCor2: anisotropic correction of beam-induced motion for improved cryo-
452 electron microscopy. *Nat Methods* 14(4):331–332.

453 40. Zhang K (2016) Journal of Structural Biology. *J Struct Biol* 193(1):1–12.

454 41. Pettersen EF, et al. (2004) UCSF Chimera--a visualization system for exploratory research and analysis. *J*
455 *Comput Chem* 25(13):1605–1612.

456 42. Grigorieff N (2007) FREALIGN: High-resolution refinement of single particle structures. *J Struct Biol*
457 157(1):117–125.

458 43. Afonine PV, Headd JJ, Adams TCTPD (2013) New tool: phenix.real_space_refine. 4:43–44.

459 44. Emsley P, Cowtan K (2004) research papers. *Acta Cryst (2004) D60, 2126-2132*
460 *[doi:101107/S0907444904019158]*:1–7.

461 45. Khayat R, et al. (2011) The 2.3-angstrom structure of porcine circovirus 2. *J Virol* 85(15):7856–7862.

462

463

464 **Figure Legends**

465 **Table 1: Statistics of cryo-EM image reconstructions and refined atomic coordinates.**

466 **Figure 1. Interaction between PCV2 and heparin sulfate conjugated chromatography sorbent.** A) Binding
467 kinetics between 370 nM (black) and 92 nM PCV2 VLP and heparin sulfate (red). B) PCV2 elutes from the
468 chromatography sorbent in the presence of increasing concentration of heparin sulfate. C) Competition assays
469 testing the ability of various GAGs and polysaccharides to displace PCV2 from the chromatography sorbent: (red)
470 dp6 heparin sulfate (6-hexose), (blue) dp10 heparin sulfate (10-hexose), (dark grey) dp20 heparin sulfate (20-
471 hexose), (black) dp36 heparin sulfate (36-hexose), (magenta) dextran sulfate 8kDa, (light grey) chondroitin
472 sulfate B, and (olive) hyaluronic acid. Error bars represent the standard deviation of three measurements.

473 **Figure 2. Cryo-EM image reconstructions of PCV2 and PCV2 liganded to heparin sulfate.** A) Cα trace of a PCV2
474 subunit with side chains shown as stick models. Overlaid onto the stick model is a mesh representation of PCV2
475 symmetrized (left) unliganded image reconstruction at 3.3Å, and (right) liganded image reconstruction at 2.8Å.
476 B) Atomic model of the image reconstructions with the atomic displacement parameters (ADP) colored from
477 blue (low ADP) to white (medium ADP) to red (high ADP). The scale on the bottom represents the absolute
478 values of the ADP. The greater white colored atoms in the liganded image reconstructions indicates atoms with
479 higher ADP, and thus a more dynamic structrue. Images generated with UCSF Chimera.

480 **Figure 3. Focused classification of the PCV2 VLP liganded to heparin sulfate image reconstruction.** Symmetry
481 expansion of 13,600 particles generates 816,000 capsid protein subunits for analysis. A) The molecular envelope
482 for a subunit is shown in green. The mask used for the classification is shown as a transparent cyan blob. B) Ten
483 classes were requested. The number of particles and resolution reported by Frealign is written below each class.
484 C) Difference peaks for each class average shown in B. There is no difference peak for Class 1. The blue patches
485 represent the molecular envelope of Arg/Lys side chains. Class numbers referred to in the text are written at
486 the bottom. Images made with UCSF ChimeraX.

487 **Figure 4. PCV2 heparin interaction and site directed mutagenesis of binding sites.** The PCV2 shell is shown as a
488 cyan cartoon ribbon. The difference peak (at 27-sigma) is shown as a grey transparent blob –low pass filtered to

489 7Å. The heparin sulfate is shown as a dark grey stick model. The solid lines represent hydrogen bonds and/or
490 salt bridges to the sulfates (red and yellow sticks) of heparin sulfate. A) Class 2 binding site. B) Class 4 binding
491 site. C) Class 6 binding site. D) Class 7 binding site. E) Class 9 binding site. F) Class 10 binding site. G) The bars
492 represent the efficiency of 370 nM mutant PCV2 VLP for binding to heparin sulfate, with wild-type (WT) VLP
493 having been normalized to 1. Some mutants did not assemble into capsids (NA). Images made with UCSF
494 Chimera, and Origin 2016.

495 **Figure 5. Occupied heparin sulfate binding sites mapped onto VLP**. The coloring scheme used is identical to
496 Figure 3. A) Models represent VLP with 20-22 binding sites occupied by heparin sulfate (20-22). B) Models
497 represent VLP with 35 binding sites occupied by heparin sulfate, D) Models represent VLP with 45-50 binding
498 sites occupied by heparin sulfate. An icosahedral cage has also been drawn for each particle. Images made with
499 UCSF Chimera.

500

501 **Table1.**

	Unliganded PCV2	PCV2 + Heparin sulfate
Image reconstruction		
Micrographs	1,149	3,725
Defocus range	-0.28 to -3.2 μm	-0.25 to -3.6 μm
Total dose	35 e- $Å^{-2}$	32 e- $Å^{-2}$
Dose rate	7.0 e^{-} $Å^{-2}$ sec^{-1}	6.4 e^{-} $Å^{-2}$ sec^{-1}
Frames	50	25
Particles extracted	54,409	166,369
Particles used for reconstruction	28,938	93,725
FSC resolution *	3.3 Å	2.8 Å
B-factor sharpening †	-152.2 $Å^2$	-122.92 $Å^2$
Atomic modeling		
CC	82%	83%
B-factor average	35.5 $Å^2$	38.1 $Å^2$
RMSD ‡	0.012	0.016
RMSD §	1.278	1.271
Molprobity ¶	1.76	1.62
EMRinger	4.89	5.02
EMDB	8939	
PDB	6DZU	

502 * Fourier shell correlation reported by Relion 2.0 using the gold standard method at a CC of 0.143.
503 † The B-factor sharpening reported by Relion 2.0 during the post-refinement process
504 ‡ The root-mean standard deviation for bonds reported by Phenix.real_space_refine
505 § The root-mean standard deviation for angles reported by Phenix.real_space_refine
506 ¶ Molprobity Overall score
507
508

Figure 1.

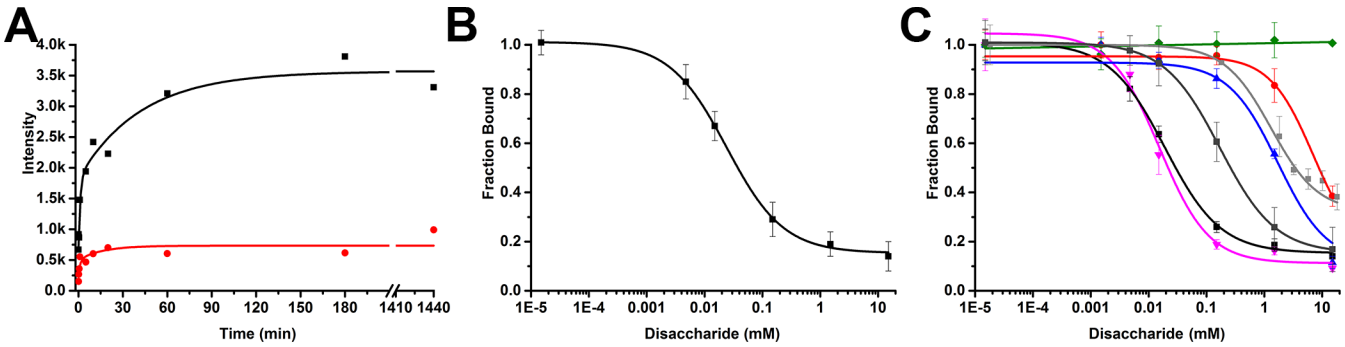
A
Intensity
4.0k
3.5k
3.0k
2.5k
2.0k
1.5k
1.0k
0.5k
0.0
0
30
60
90
120
150
180
1410
1440
Time (min)
B
Fraction Bound
1.0
0.8
0.6
0.4
0.2
0.0
1E-5
1E-4
0.001
0.01
0.1
1
10
Disaccharide (mM)
C
Fraction Bound
1.0
0.8
0.6
0.4
0.2
0.0
1E-5
1E-4
0.001
0.01
0.1
1
10
Disaccharide (mM)

Figure 2.

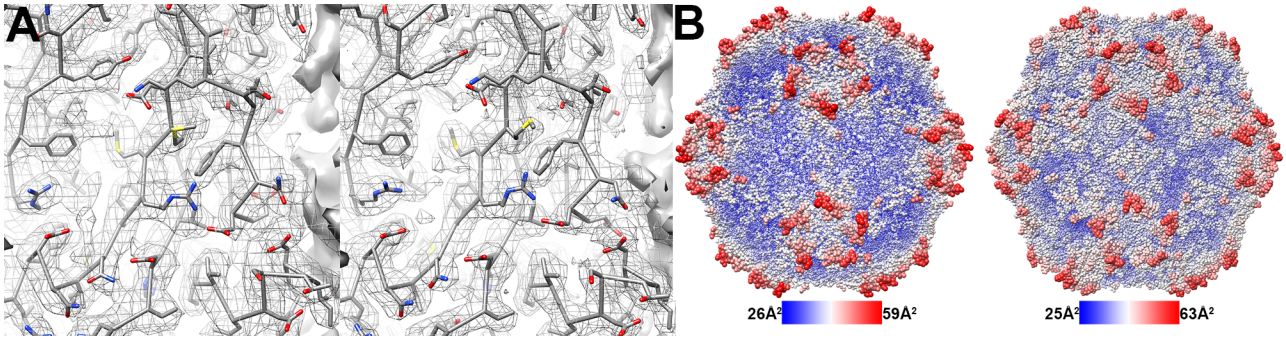

Figure 3.

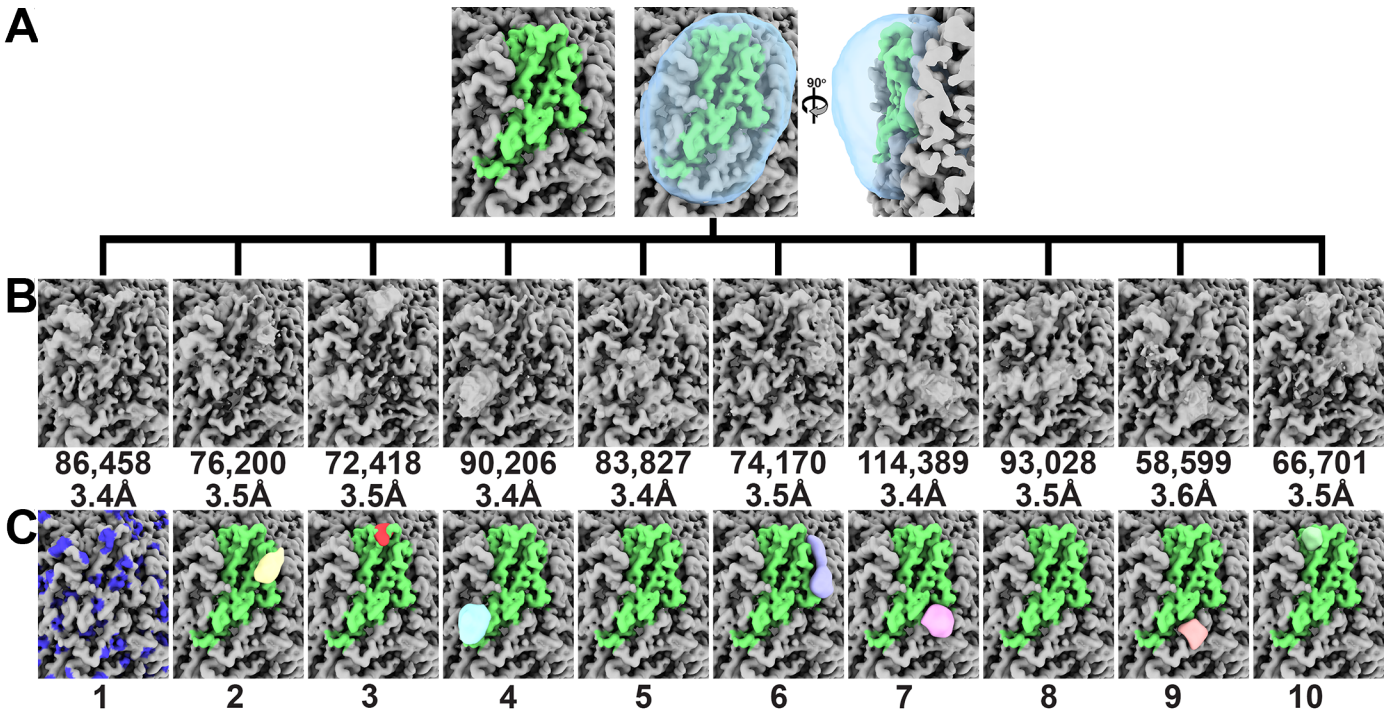
A
90°
B
86,458
3.4Å
76,200
3.5Å
72,418
3.5Å
90,206
3.4Å
83,827
3.4Å
74,170
3.5Å
114,389
3.4Å
93,028
3.5Å
58,599
3.6Å
66,701
3.5Å
C
1
2
3
4
5
6
7
8
9
10

Figure 4.

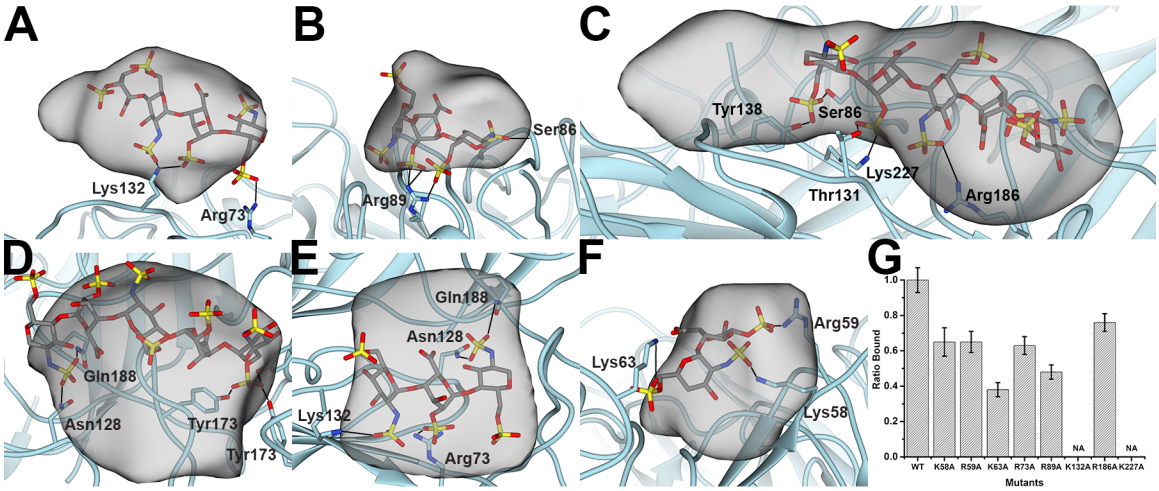
A
Lys132
Arg73
B
Ser86
Arg89
C
Tyr138
Ser86
Lys227
Thr131
Arg186
D
Gln188
Asn128
Tyr173
Tyr173
E
Gln188
Asn128
Lys132
Arg73
F
Arg59
Lys63
Lys58
G
Ratio Bound
1.0
0.8
0.6
0.4
0.2
0.0
WT
K58A
R59A
K63A
R73A
R89A
K132A
R186A
K227A
NA
NA
Mutants

Figure 5.

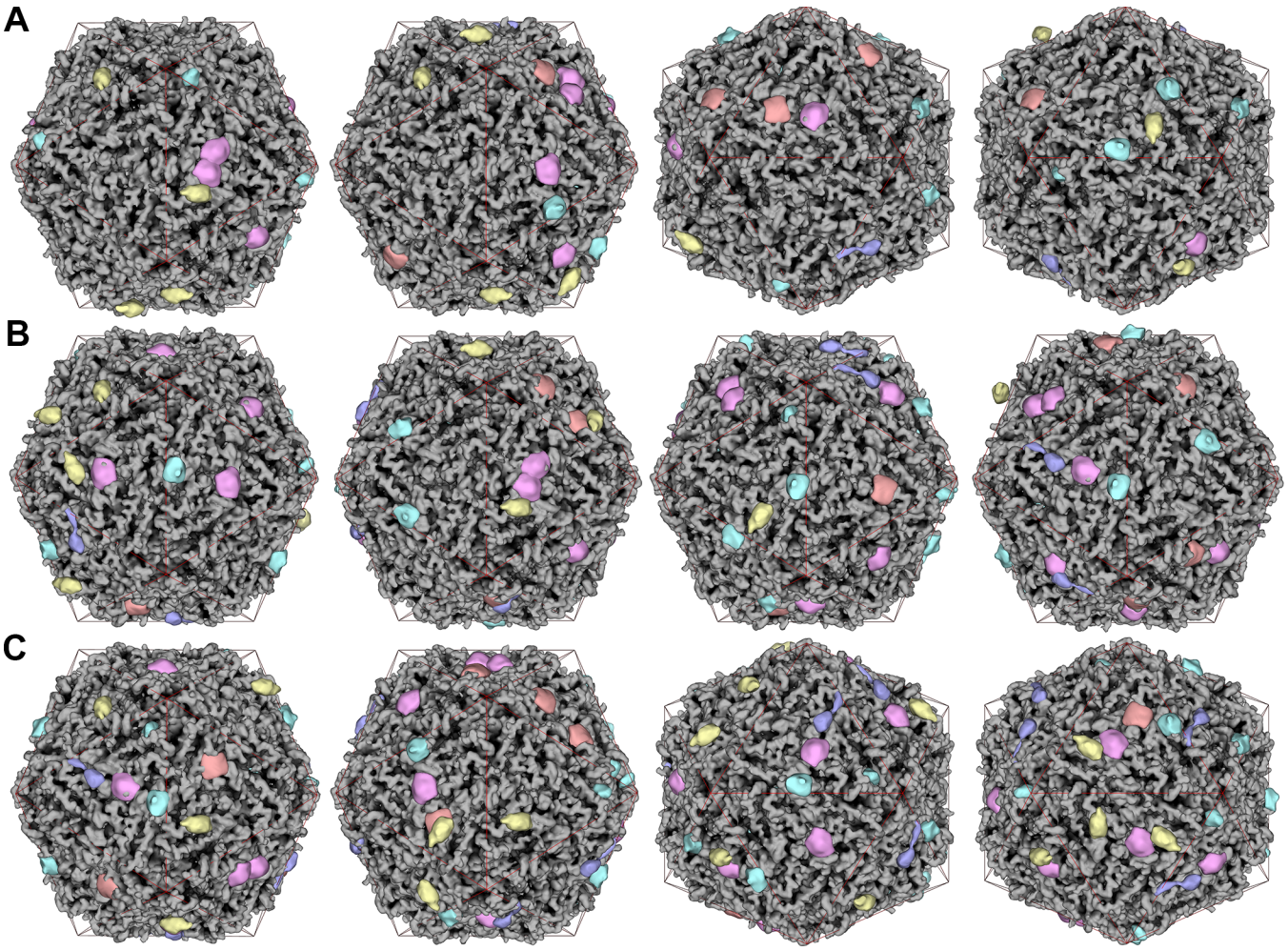

525 **Supplemental Information**

526 **Figure S1. Heparan sulfate and heparin sulfate**. Top) Cartoon representation of the NS and NA domains of a
527 heparan sulfate glycosaminoglycan chain. The NS domain is composed of 3-8 repeating disaccharides, and the
528 NA domain is composed of 2-12 repeating disaccharide. Bottom) Chemical structure of the heparan sulfate and
529 heparin sulfate repeating disaccharides. The repeating disaccharide of the heparan sulfate NS domain is similar
530 to the repeating disaccharide of heparin sulfate.

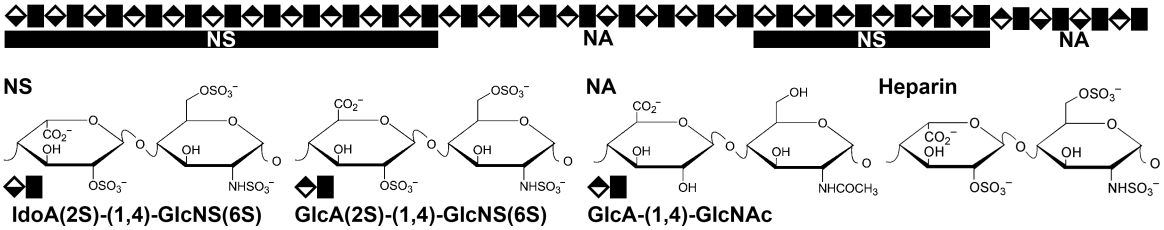

531

532

533

Figure S2. SDS-PAGE densitometry of PCV2 VLP heparin binding interaction. Images represent the interaction between PCV2 VLP and HyperD™ chromatography sorbent. The contrast of each digitized SDS-PAGE was scaled to enhance the signal for visualization. This modification does not affect the intensity reported by the Image Studio™ software used for the analysis. The numbers above each band represent the intensity corrected by background subtraction within each box. A) Linear response curve of the LI-CORR Odyssey CLX to increasing amount of PCV2 capsid protein, indicating that intensity is directly correlated to protein content. B) Binding kinetics of 370 nM and 97 nM VLP demonstrating that the signal from 370 nM produces a robust readout (Figure 1A). Elution of VLP from the sorbent with increasing heparin concentration (Figure 1B). Binding efficiency of *in vitro* assembled wild-type, K58A, R59A, K63A, R73A, R89A, and R186A capsids (Figure 4). GAG competition assay representatives of: C) 6-hexose, D) 10-hexose, E) 20-hexose, F) 36-hexose heparin, G) chondroitin sulfate B, H) dextran sulfate 8kDa, and I) hyaluronic acid. The plots for panels C-I are representatives of Figure 1C.

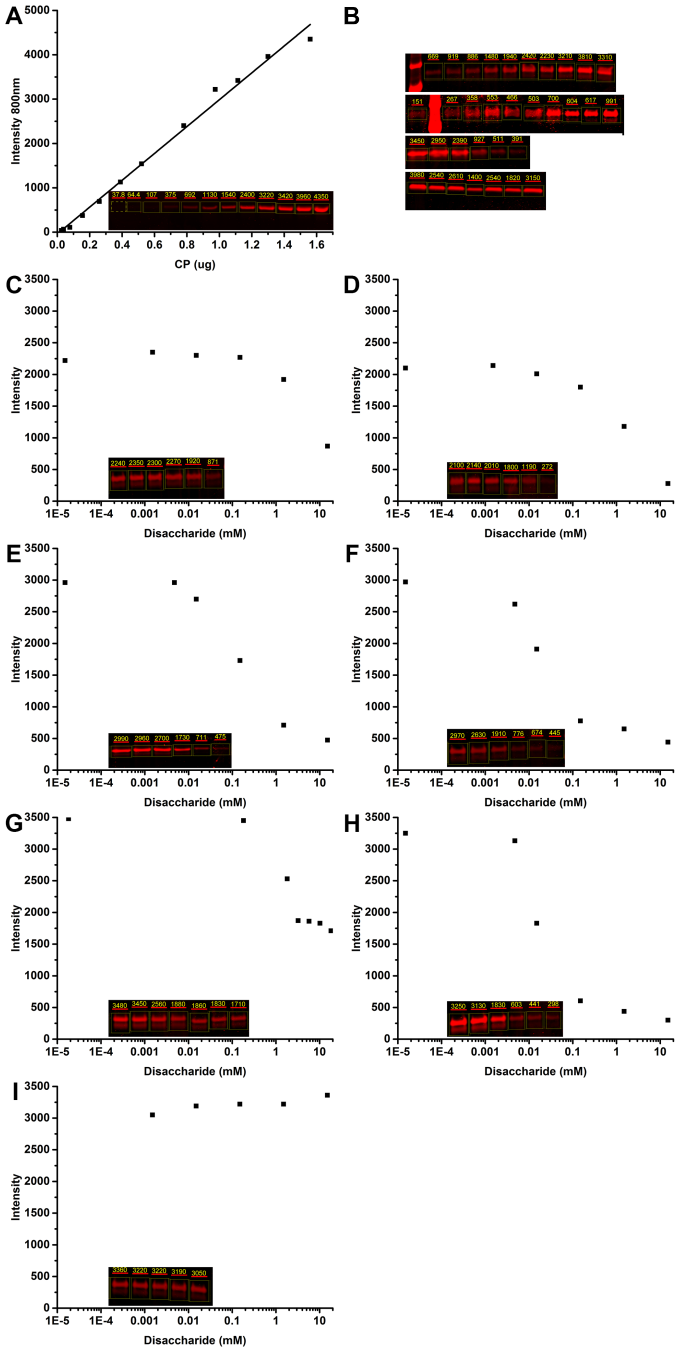

547 **Figure S3. VLP assembly of mutant capsid proteins.** Size exclusion chromatography profile of an *in vitro*
548 assembled PCV2 VLP and a corresponding electron microscope micrograph of the negative stained wild-type
549 VLP.

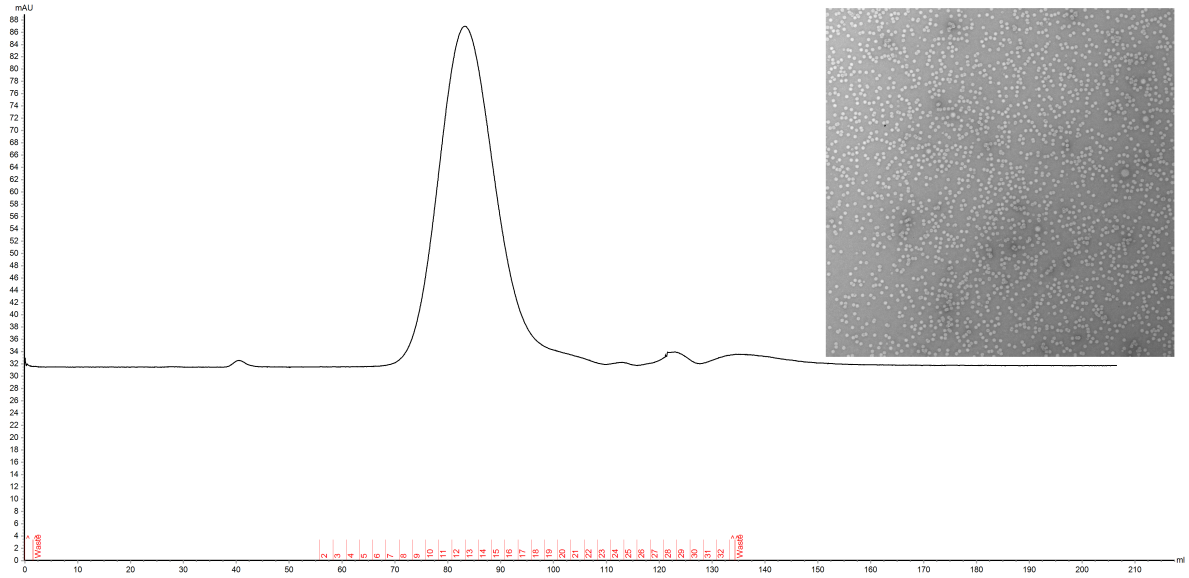

550

551

552 **Figure S4. Occupied heparin sulfate binding sites on PCV2 VLPs.** The distribution follows a Gaussian profile with
553 a minimum of 20, a mode of 35, and a maximum of 47 binding sites occupied on individual VLPs.

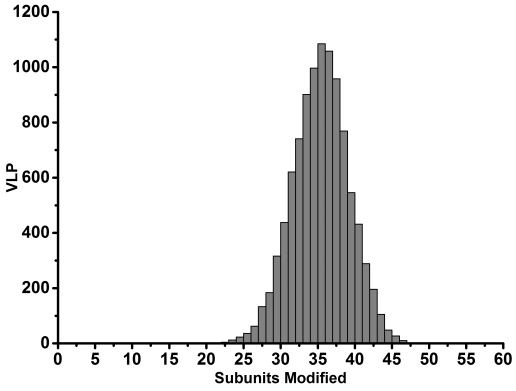

554

555

556